79-4039

Computation of Three-Dimensional Potential Flow Using Surface Vorticity Distribution

Pradeep Raj* and Robin B. Gray†
Georgia Institute of Technology, Atlanta, Ga.

An iterative method is developed using incompressible potential flow theory to compute three-dimensional velocity and pressure distributions on the surface of thick wings. The mathematical formulation is illustrated for a semi-infinite circular cylinder having a hemispherical tip. The procedure starts from a specified two-dimensional vorticity distribution on the entire body and converges in three iterations to the three-dimensional distribution on the tip which merges smoothly with the two-dimensional one further inboard. The finite-element approach used here gives a continuous distribution of vorticity which is directly equivalent to the surface velocity distribution. The present method involves repeated use of the Biot-Savart law to relax the surface vorticity strength in successive iterations; whereas the more commonly used integral equation formulation requires solving a large matrix which is usually not well behaved for the surface vorticity model. A modification of the method is applied to compute the nonlifting flow on a semi-infinite NACA 0012 wing with a half-body-of-revolution tip and a NACA 0012 wing with an aspect ratio of three. The chordwise pressure coefficient distributions are presented for representative spanwise locations for all of the cases.

Nomenclature

AR	= aspect ratio of a wing
c	= chord
C_p	= pressure coefficient
C_1, C_2, C_3	= direction cosines with respect to X, Y, Z axes, respectively, of a vector tangent to the surface at a control point
i,j,k	= unit vectors along X, Y, Z axes, respectively
k,l,m	= stations on the body surface used to define surface elements (see Fig. 1)
K,L,M	= total number of k,l,m stations, respectively
t_1, t_2, t_3	= direction cosines of the tangential induced velocity vector on the body surface
V	= total fluid velocity
x,y,z	= Cartesian coordinates of a point
X,Y,Z	= Cartesian coordinate system
α,β	= spanwise and chordwise components of the surface vorticity vector, respectively
γ	= surface vorticity strength
ψ	= angular location of an m station on the tip

Subscripts

i	= quantities associated with ith control point
k,l,m	= quantities associated with kth, lth, and mth stations, respectively
L	= lower surface
T	= tip
U	= upper surface
α	= quantities associated with α-type vorticity
β	= quantities associated with β-type vorticity
∞	= freestream

Introduction

ONE of the problems of continuing interest to aerodynamicists is concerned with the development of more accurate and efficient methods for the determination of pressure and velocity distributions on arbitrarily shaped bodies. Ideally, one would like to solve the Navier-Stokes equations but the task is made quite tedious by the nonlinear nature of the equations. However, the incompressible potential flow approach not only affords considerable mathematical simplification, but the results also agree very well with low-speed real flows for a large class of bodies and flow configurations. The essential simplicity stems from the fact that the velocity fields are completely determined by solutions of Laplace's equation subject to appropriate boundary conditions. The equation of motion is used only to obtain the pressure field once the velocity field is known.

Even though Laplace's equation is one of the simplest and best known of all the partial differential equations, the number of exact analytical solutions is far too small to suit wide practical applications. The primary difficulty lies in satisfying the boundary conditions for a prescribed surface. This can be alleviated to some extent by introducing suitable approximations into the formulation. However, the attainable accuracy for the approximate solutions is limited and usually there are restrictions attached to the type of body on which the flow can be computed. For a body of arbitrary shape, the exact numerical methods have been steadily gaining importance in the past decade with the rapid advances in high-speed digital computers. In these methods, the analytical formulation is exact and the computational errors can, in principle, be made as small as desired by sufficiently refining the numerical procedure.

The more commonly used exact numerical method is based on an integral equation formulation. This involves expressing the solution of Laplace's equation as an integral over the bounding surface for an unknown distribution of surface singularities (sources, doublets, and vortices).[1] One of the most important advantages of this procedure is that the solution can be computed on the body surface without considering the remainder of the flowfield. Hess and Smith[2] successfully apply this formulation using surface source distributions for a variety of bodies. The bounding surface is approximated by plane rectangular surface elements over each of which the source density is assumed to be constant. Hess[3,4] presents improvements to the basic approach for axisymmetric and three-dimensional bodies. A vorticity distribution is, of course, superimposed on the source distribution to provide the circulation for lifting flows. Woodward[5] uses the

Received April 21, 1978; revision received Aug. 14, 1978. Copyright © American Institute of Aeronautics and Astronautics, Inc., 1978. All rights reserved.

Index categories: Aerodynamics; Computational Methods.

*Graduate Research Assistant; presently Assistant Professor, Department of Aerospace Engineering, Iowa State University, Ames, Iowa. Member AIAA.

†Regents' Professor and Associate Director, School of Aerospace Engineering. Member AIAA.

source and vortex distributions for wing-body-tail configurations; the former is used on the body panels and the latter on the wing and tail panels. Pien[6] points out a disadvantage of the surface source method, namely, the difficulties in computing the velocity and pressure even after the source densities are determined, and advocates use of a doublet distribution. Summa[7] developed a method based on a step doublet distribution over elements of a discrete set of approximate quadrilateral elements on the surface. The use of a vorticity distribution suggested by Prager[8] has attracted only limited attention especially for three-dimensional flows. Kress[9] deals explicitly with the case of nonsimply connected bodies, such as a torus, and Klein and Mathew[10] have developed a method for axisymmetric flows. Grodtkjaer[11] presents a direct integral equation method for three-dimensional flows which involves the formulation of a pair of singular integral equations of the second kind with surface velocity components as unknowns. The integral equations are approximated by a set of linear equations which are solved numerically. The results for ellipsoids are presented in Grodtkjaer's paper.

The use of vorticity as the surface singularity has certain advantages over other methods which deserve careful attention. This is the only procedure which gives the surface velocity directly as the solution of the equation. This follows from the fact that the discontinuity in the tangential velocity is the local vorticity strength and, if the interior velocity is zero, then the surface vorticity strength is equivalent to the surface velocity. The vorticity also represents an ideal model of the physically observed phenomenon as some vorticity is unavoidably required to provide circulation for lifting flows. The authors, therefore, find it more natural to formulate the entire problem of incompressible, inviscid flow in terms of vorticity.

An integral equation formulation using surface vorticity distribution for the computation of three-dimensional velocity fields poses the following difficulty. The surface vorticity distribution coupled with the zero-normal-flow boundary condition leads to a Fredholm integral equation of the first kind. This equation has to be numerically solved for an arbitrary bounding surface and the usual procedure is to approximate the integral equation by a set of linear algebraic equations. However, the diagonal entries of the resulting coefficient matrix are not necessarily larger than the other entries. This can be a crucial factor in the numerical matrix-solution method. The large size of the matrix as required for a sufficiently detailed and accurate determination of the flowfield further aggravates the difficulties. In this paper, instead of the integral equation formulation, an alternate method based on a simple iterative procedure is presented.

Development of the Iterative Procedure

Basic Concept

The formulation of the iterative procedure is best illustrated by considering a semi-infinite body. For clarity of sequences in the development, consider a semi-infinite circular cylinder of unit radius having a hemispherical tip. The flow on this body, placed with its axis perpendicular to the freestream is essentially two-dimensional except for a limited zone of three-dimensional flow near the tip. The iterative procedure starts with the specification that the initial vorticity strength at a chordwise location on the entire body is the same as the corresponding value for a two-dimensional circular cylinder. (In other words, the two-dimensional vorticity distribution that occurs at a great distance inboard on the cylinder is maintained unchanged to and around the tip thereby satisfying continuity of the vorticity.) Obviously, this does not conform to the actual distribution near the tip. The initial distribution, therefore, has to be adjusted such that the final three-dimensional vorticity distribution on the tip merges smoothly with the two-dimensional distribution further inboard. The underlying concept of the iterative procedure is to successively relax the surface vorticity distribution under its own influence until the proper distribution is obtained on the surface. This is accomplished by the following finite-element approach.

The body surface is first divided into a finite number of elements, each containing a control point where the tangential component of the induced velocity due to all the elementary distributions is computed using the Biot-Savart law. This is added to the local tangential component of the freestream to give the mean tangential velocity of the surface vorticity sheet which is one-half of the local velocity[12] and equivalently, half of the vorticity strength. The local vorticity vector is, of course, perpendicular to the velocity vector. The computed value of the surface vorticity will not, in general, agree with the initial value in magnitude or direction. The initial values of the surface vorticity are now replaced by the computed values at the control points and the vorticity distribution is assumed to vary linearly between any two control points. Thus, the body has a piecewise linear, continuous vorticity distribution on its surface which is different from the initial one (but not necessarily the correct distribution). The next step is to compute the induced velocities, consequently the vorticity strengths, at the control points as resulting from the modified surface vorticity distribution. The new results are then compared with the previous values. If the agreement is not within prescribed limits, the computed vorticity distribution replaces the previous one and further relaxation continues. In principle, the procedure can be carried out until the difference in the values of the surface vorticity for two successive iterations is insignificant. The results, however, show that good convergence is obtained in about three to four iterations for nonlifting flows.

It is important to note that the local vorticity vector is completely specified by a pair of orthogonal vectors on the surface which are designated α-type and β-type. The initial two-dimensional vorticity distribution is entirely α-type. The β-type is needed, in addition to the α-type, near the tip to account for the three-dimensionality. The net surface vorticity strength, δ, is obtained from

$$\delta = (\alpha^2 + \beta^2)^{1/2} \tag{1}$$

Surface Elements

On the cylinder ($y \leq 0$), any plane parallel to the Y-Z plane intersects the surface along a semi-infinite straight line which is called a k station (Fig. 1). A plane parallel to the X-Z plane intersects the cylinder along a circle of unit radius which is called an l station. The k stations, the l stations, and the curved body surface form the elements on the cylindrical body. On the hemispherical tip, mutually orthogonal longitudes and latitudes are drawn as follows. A plane parallel to the Y-Z plane intersects the hemisphere along a semicircle which corresponds to a latitude and defines a k station. A radial plane containing the X axis and inclined at an angle ψ to the X-Z plane intersects the hemisphere along a unit circle which corresponds to a longitude and defines an m station. The k stations, the m stations, and the curved surface form the elements on the hemisphere which is mathematically expressed as

$$(x-1)^2 + y^2 + z^2 = 1 \tag{2}$$

All of the elements on the body are curved surfaces of different shapes and sizes. The procedure offers enough flexibility for varying the number and sizes of the elements. On each element, the geometric midpoint is designated to be a control point.

Zeroth Iteration

Initially, the chordwise vorticity distribution on the body is identical at every l and m station. The vorticity on the hemispherical tip is composed of semicircular filaments lying

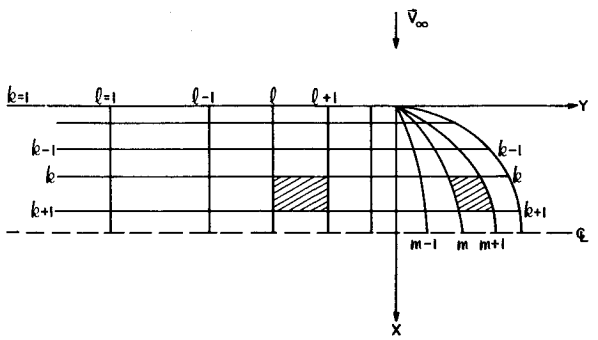

Fig. 1 Semi-infinite circular cylindrical body with a hemispherical tip.

along the latitudes and the distribution on the circular cylindrical section of the body is constituted of semi-infinite, straight-line filaments. The total induced velocity, V_i, at the ith control point is the sum of the contributions V_U and V_L from the upper and lower surface vorticity distributions on the cylindrical portion ($y \leq 0$), respectively, and the contribution V_T from the vorticity distribution on the hemispherical tip, i.e.,

$$V_i = V_U + V_L + V_T \tag{3}$$

where

$$V_{U,L} = \pm \frac{1}{4\pi} \sum_{k=1}^{K} \int_{x_k}^{x_{k+1}} G(x)\,(1 - y_i r^{-1}) J_1 r^{-2} m_z \mathrm{d}x \tag{4}$$

$$G(x) = \gamma_k + (x - x_k)\Delta_k \gamma_k / \Delta_k x_k$$

$$J_1 = (z_i - z) C_1 - (x_i - x) C_3$$

$$r = \{ (x_i - x)^2 + (z_i - z)^2 \}^{1/2}$$

$$m_z = \{ 1 + (\mathrm{d}z/\mathrm{d}x)^2 \}^{1/2}$$

$$z = \pm (2x - x^2)^{1/2} \qquad (y \leq 0)$$

$$\Delta_k = E_k^{+1} - 1 \qquad E_k^{+1} x_k = x_{k+1}$$

and

$$V_T = \frac{1}{4\pi} \sum_{k=1}^{K} \int_{x_k}^{x_{k+1}} \int_0^{\pi} G(x) J_2 R^{-3} \lambda(x) m_\lambda \mathrm{d}\epsilon \mathrm{d}x \tag{5}$$

where $G(x)$ is defined following Eq. (4) and

$$R = \{ r^2 + (y_i - y)^2 \}^{1/2}$$

$$J_2 = \{ (z_i - z)\cos\epsilon + (y_i - y)\sin\epsilon \} C_1$$

$$- (x_i - x)\,(C_2 \sin\epsilon + C_3 \cos\epsilon)$$

$$m_\lambda = \{ 1 + (\mathrm{d}\lambda/\mathrm{d}x)^2 \}^{1/2}$$

$$\lambda(x) = (2x - x^2)^{1/2}$$

$$y = \lambda(x)\sin\epsilon \qquad z = \lambda(x)\cos\epsilon$$

When two signs appear for a term, the upper sign corresponds to the upper surface and the lower one to the lower surface.

It is expected and borne out by the results of the zeroth iteration that the α-type vorticity distribution at the l stations approaches the corresponding two-dimensional distribution at a few chord lengths inboard from the tip. The value of the β-type vorticity approaches zero simultaneously. There is then a cutoff station, $l = 1$, inboard of which the flow is essentially two-dimensional and represented entirely by the α-type vorticity. On and near the tip, the vorticity distribution is composed of both the α-type and the β-type.

First Iteration

The results of the zeroth iteration provide the input surface vorticity distribution for the first iteration. The computation of the induced velocities due to the new system is carried out by using the Biot-Savart law. It is convenient to consider the contributions of the α-type and the β-type vorticity distributions separately as follows:

The induced velocity at the ith control point due to the α-type vorticity distribution is the sum of the contributions of the upper ($z \geq 0$) and lower ($z \leq 0$) surfaces of the cylindrical portion ($y \leq 0$) of the body and the hemispherical tip, that is,

$$V_{i_\alpha} = V_{U_\alpha} + V_{L_\alpha} + V_{T_\alpha} \tag{6}$$

Here

$$V_{U_\alpha, L_\alpha} = \pm \sum_{k=1}^{K} \Delta V_k \pm \sum_{k=1}^{K} \sum_{l=1}^{L} \Delta V_{kl}$$

The term ΔV_k expresses the contribution of the entire strip extending to infinity inboard of the cutoff station, y_l, with $x_k \leq x \leq x_{k+1}$ and is expressed by

$$\Delta V_k = \frac{1}{4\pi} \int_{x_k}^{x_{k+1}} G(x) \{ 1 + (y_l - y_i) R^{-1} \} J_1 r^{-2} m_z \mathrm{d}x \tag{7}$$

The term ΔV_{kl} is the contribution of the element lying between the stations l and $l+1$ and the stations k and $k+1$ (see cross-hatched area in Fig. 1). Using the Biot-Savart law, this term can be expressed as

$$\Delta V_{kl} = \frac{1}{4\pi} \int_{x_k}^{x_{k+1}} \{ a_l J_3 - b_l J_4 + (a_2 J_3 - b_2 J_4) x \} J_1 m_z \mathrm{d}x \tag{8}$$

where J_1 and m_z are defined following Eq. (4) and

$$J_3 = \{ (y_{l+1} - y_i)/\mathrm{d}_{l+1} - (y_l - y_i)/\mathrm{d}_l \} r^{-2}$$

$$J_4 = \{ (a - y_i y_{l+1})/\mathrm{d}_{l+1} - (a - y_i y_l)/\mathrm{d}_l \} r^{-2}$$

$$a = r^2 + y_i^2$$

$$\mathrm{d}_{l+1} = \{ a - 2y_i y_{l+1} + y_{l+1}^2 \}^{1/2}$$

$$\mathrm{d}_l = \{ a - 2y_i y_l + y_l^2 \}^{1/2}$$

$$a_l = (f_l y_{l+1} - f_{l+1} y_l)/\Delta_l y_l \qquad b_l = \Delta_l f_l / \Delta_l y_l$$

$$a_2 = (e_l y_{l+1} - e_{l+1} y_l)/\Delta_l y_l \qquad b_2 = \Delta_l e_l / \Delta_l y_l$$

$$e_l = \Delta_k \gamma_{k,l} / \Delta_k x_k$$

$$f_l = (\gamma_{k,l} x_{k+1} - \gamma_{k+1,l} x_k)/\Delta_k x_k$$

The double integral in the following equation represents the contribution to the induced velocity component at the ith control point from the surface element on the tip between the stations k and $k+1$ and m and $m+1$. The total contribution is

$$V_{T_\alpha} = \frac{1}{4\pi} \sum_{k=1}^{K} \sum_{m=1}^{M} \int_{x_k}^{x_{k+1}} \int_{\psi_m}^{\psi_{m+1}}$$

$$(a_3 x + a_4) J_2 R^{-3} \lambda(x) m_\lambda \mathrm{d}\epsilon \mathrm{d}x \tag{9}$$

where m_λ, $\lambda(x)$, R, and J_2 are defined following Eq. (5) and

$$a_3 = \{\Delta_k(\lambda_k g_{k,m})\sin\epsilon + \Delta_k h_{k,m}\}/\Delta_k x_k$$

$$a_4 = \{(\lambda_k g_{k,m} x_{k+1} - \lambda_{k+1} g_{k+1,m} x_k)\sin\epsilon + (h_{k,m} x_{k+1} - h_{k+1,m} x_k)\}/\Delta_k x_k$$

$$g_{k,m} = \Delta_m \gamma_{k,m}/\Delta_m y_{k,m}$$

$$h_{k,m} = (\gamma_{k,m} y_{k,m+1} - \gamma_{k,m+1} y_{k,m})/\Delta_m y_{k+1,m}$$

$$y_{k,m} = \lambda_k \sin\psi_m = \lambda(x_k)\sin\psi_m$$

The β-type vorticity distribution is confined to the hemispherical tip and the region between the tip and the cutoff station. The tangential induced velocity, $V_{i\beta}$, is the sum of the contributions from the upper and lower surface vorticity distributions on the cylindrical portion and from the hemispherical tip, that is,

$$V_{i\beta} = V_{U\beta} + V_{L\beta} + V_{T\beta} \tag{10}$$

Here

$$V_{U\beta, L\beta} = \frac{1}{4\pi}\sum_{k=1}^{K}\sum_{l=1}^{L}\int_{x_k}^{x_{k+1}} (I_1 + I_2 + I_3) m_z \, dx \tag{11}$$

where m_z is defined following Eq. (4), J_3 and J_4 following Eq. (8), and

$$I_1 = a_6 b_6 J_3 \qquad I_2 = -(a_5 b_6 + a_6 b_5) J_4$$

$$I_3 = a_5 b_5 \{[y_{l+1}(y_i^2 - a) - a y_i]/d_{l+1} - [y_l(y_i^2 - a) - a y_i]/d_l\} r^{-2} + a_5 b_5 \ell n[(y_{l+1} - y_i + d_{l+1})/(y_l - y_i + d_l)]$$

$$a_5 = \mp C_1 \sin\theta \pm C_3 \cos\theta$$

$$a_6 = C_2\{\mp (x_i - x)\sin\theta \pm (z_i - z)\cos\theta\} - y_i a_5$$

$$b_5 = \{\Delta_k g_{k,l} x + (x_{k+1} g_{k,l} - x_k g_{k+1,l})\}/\Delta_k x_k$$

$$b_6 = \{\Delta_k h_{k,l} x + (x_{k+1} h_{k,l} - x_k h_{k+1,l})\}/\Delta_k x_k$$

$$g_{k,l} = \Delta_l \gamma_{k,l}/\Delta_l y_l$$

$$h_{k,l} = (\gamma_{k,l} y_{l+1} - \gamma_{k,l+1} y_l)/\Delta_l y_l$$

$$\tan\theta = dz/dx$$

and

$$V_{T\beta} = \frac{1}{4\pi}\sum_{k=1}^{K}\sum_{m=1}^{M}\int_{x_k}^{x_{k+1}}\int_{\psi_m}^{\psi_{m+1}} (a_3 x + a_4) \times (I_1 + I_2 + I_3) R^{-3} \lambda(x) m_\lambda \, d\epsilon \, dx \tag{12}$$

where

$$I_1 = -(x_i - x)(C_2\cos\epsilon - C_3\sin\epsilon)\sin\theta$$

$$I_2 = -(y_i - y)(C_3\cos\theta - C_1\sin\theta\cos\epsilon)$$

$$I_3 = -(z_i - z)(C_1\sin\theta\sin\epsilon - C_2\cos\theta)$$

$$\tan\theta = d\lambda/dx$$

and the definitions of the other variables are given following Eq. (9).

The net tangential induced velocity $V_i = V_{i\alpha} + V_{i\beta}$, is added to the corresponding tangential component of the freestream velocity to obtain the α and β components of vorticity. The computed values define a new system of surface vorticity distribution to be used for the next iteration. The procedure, including all equations, is identical to that of the first iteration, Eqs. (6-12).

Numerical Procedure

Before starting the computations for the zeroth iteration, the upper and lower surfaces of the cylindrical portion of the body are each divided into 30 semi-infinite strips. There are correspondingly 30 semicircular segments on the hemispherical tip. The initial chordwise vorticity strength distribution at every spanwise location is the same as the two-dimensional distribution on a circular cylinder.[13] The induced velocity at any point on the body due to this system of vorticity is obtained by numerically evaluating the integrals in Eqs. (4) and (5) by using Simpson's rule. When the point lies on a strip whose contribution is being evaluated, the integrand exhibits the indeterminate (0/0) form. The integral can still be evaluated numerically by using a combination of Simpson's rule and the trapezoidal rule.[14] The latter is used very close to the singular point where the slope of the integrand with respect to the X axis becomes large. The contributions of the small intervals on each side of the singular point steadily reduce as this point is approached.

The location of the cutoff station, $l=1$, is found to be approximately five chord lengths inboard from the $y=0$ plane. The intervening distance is divided into 10 parts giving rise to 11 l stations. On the tip, 13 m stations at 15 deg intervals are selected. At the control point on each of the surface elements, the α- and β-type vorticity strengths are computed. These results define the input vorticity distribution for the first iteration.

The tangential induced velocity at any control point due to the input vorticity distribution is obtained by numerical evaluation of the integrals in Eqs. (7-9) and Eqs. (11) and (12) using Simpson's rule. The singular control points where the integrand exhibits an indeterminate form are handled as previously described. The induced velocity components are added to the appropriate freestream component to define the α- and β-type of vorticity strengths which define the input for the next iteration. The numerical procedure remains unchanged for successive iterations.

Results

The iterative procedure is carried out to three complete iterations after the zeroth. The results show that the values of the surface vorticity strength change by smaller amounts with each iteration. The maximum change is obtained between the initial two-dimensional distribution and the results of the zeroth iteration and may be as much as 50% based on a freestream value of unity. The results of the first iteration differ from those of the third iteration by an amount which is

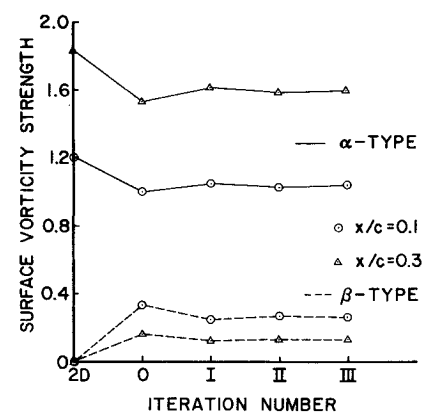

Fig. 2 Typical damped oscillatory pattern of convergence for surface vorticity strength on a semi-infinite circular cylindrical body with a hemispherical tip, $y/c = 0$.

Table 1 Variation of the circumferential velocity component on the semi-infinite circular cylindrical body in a crossflow $V = V_\alpha|_{\theta=\pi/2}\sin\theta$; V_α computed by present method

		$y/c=-0.5$		$y/c=-0.2$		$y/c=0.0$	
x/c	$\sin\theta$	V	V_α	V	V_α	V	V_α
0.025	0.3122	0.5894	0.5896	0.5681	0.5685	0.5431	0.5426
0.1	0.6	1.1327	1.1328	1.0919	1.0922	1.0437	1.0418
0.2	0.8	1.5103	1.5104	1.4558	1.4558	1.3916	1.3888
0.3	0.9165	1.7303	1.7304	1.6678	1.6676	1.5942	1.5944
0.4	0.9798	1.8498	1.8498	1.783	1.7826	1.7044	1.7052
0.5	1.0	1.8879	1.8879	1.8198	1.8198	1.7395	1.7395

Table 2 Variation of the axial velocity component on the surface of the circular cylindrical body in a crossflow $V = V_\beta|_{\theta=0}\cos\theta$; V_β computed by present method

		$y/c=-0.5$		$y/c=-0.2$		$y/c=0.0$	
x/c	$\cos\theta$	V	V_β	V	V_β	V	V_β
0.025	0.95	0.07738	0.0774	0.1581	0.1582	0.3190	0.3198
0.1	0.8	0.06512	0.06524	0.1331	0.1334	0.2686	0.2698
0.2	0.6	0.04884	0.0489	0.09984	0.1001	0.2015	0.2026
0.3	0.4	0.03256	0.0326	0.06656	0.0668	0.1343	0.1354
0.4	0.2	0.01628	0.01632	0.03328	0.0334	0.0672	0.0676
0.5	0.0	0.0	0.0	0.0	0.0	0.0	0.0

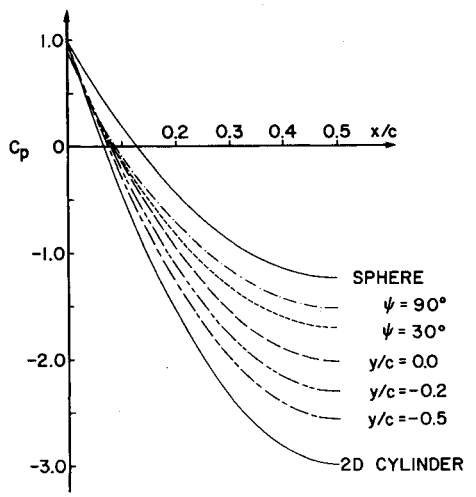

Fig. 3 Chordwise pressure coefficient distributions on a semi-infinite circular cylindrical body with a hemispherical tip.

approximately 5% and less, whereas the difference in the results of the second and third iteration is less than 2%. The results of a fourth iteration, carried out only for the α-type, differ from the third iteration by less than 1%. This led to the conclusion that the results of the third iteration may be considered as the converged solution. An interesting feature of these results is the damped oscillatory pattern of convergence as shown in Fig. 2.

A check on the accuracy of the results is provided by the values of the normal component of the total velocity vector computed for a set of representative control points. Theoretically, the normal component should be zero on the surface. In the present case, the values of this component are found to be less than 1% of the freestream value of unity. Moreover, the values of the normal velocity component steadily reduce with each successive iteration.

An added measure of confidence in the results is provided by the following observation. The case under consideration is one of an axisymmetric body in a cross-flow. Lotz[15] pointed out that the dependence of all quantities on a circumferential location is known in advance for an axisymmetric body immersed in a uniform flow which is directed normal to the body's axis of symmetry. Then, the axial and the radial velocity components vary as $\cos\theta$, the quantity itself being characterized by its value at $\theta = 0$ (at a point in the X-Y plane). The circumferential velocity component varies as $\sin\theta$, the quantity being characterized by its value for $\theta = \pi/2$. In Tables 1 and 2, the variations of the circumferential and the axial velocity components as required by the previous observation are compared with the corresponding values computed by the present method. A good agreement is noted for all the representative points on the surface.

The chordwise pressure coefficient distribution on the upper surface of the semi-infinite circular cylindrical body at five stations is presented in Fig. 3. Owing to the symmetry of the body about the centerline, only the variation between the leading edge and the midchord is shown. For the purpose of comparison, the chordwise C_p distribution for a two-dimensional circular cylinder and for a sphere are also plotted. The curves clearly show the three-dimensional relief effect as the hemispherical tip is approached from inboard where the flow is essentially two-dimensional.

Modified Iterative Procedure

Semi-Infinite Symmetrical Wing

The iterative procedure just described for a semi-infinite circular cylindrical body is applied to compute the nonlifting flowfield on a semi-infinite NACA 0012 wing with a half-body-of-revolution tip. The problems are identical, both conceptually and in mathematical details, except that the geometry of the airfoil cross section, $z = z(x)$, is expressed by a different formula.[16] The cutoff station for the wing is found to be at one chord length inboard of the tip. The k stations are relatively closely spaced near the leading edge and the trailing edge as the two-dimensional results show a relatively rapid variation of vorticity in these regions. The locations of the l stations are also dictated by the fact that the influence of the tip to render the flow three-dimensional reduces rapidly as the distance from the tip increases inboard. The iterative procedure is started by wrapping the wing with a vorticity sheet whose chordwise strength distribution corresponds to the two-dimensional one.[13] The results for four complete iterations show a converging trend, as shown in Fig. 4. More interestingly, a damped oscillatory pattern of convergence, which is quite similar to that found for the circular cylinder, is observed. This observation suggests the following modification to the basic procedure so that the rate of convergence could be improved.

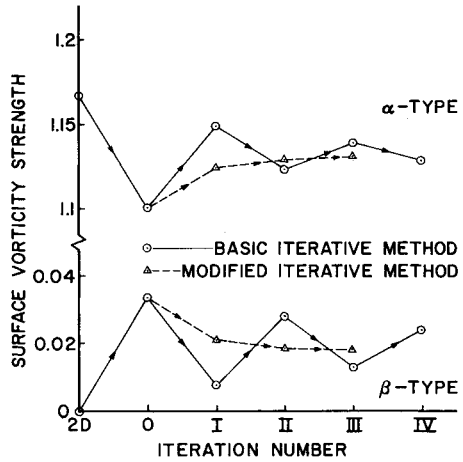

Fig. 4 Comparison of oscillatory pattern of convergence of basic and modified iterative methods for a semi-infinite NACA 0012 wing, $x/c = 0.25$, $y/c = -0.1$.

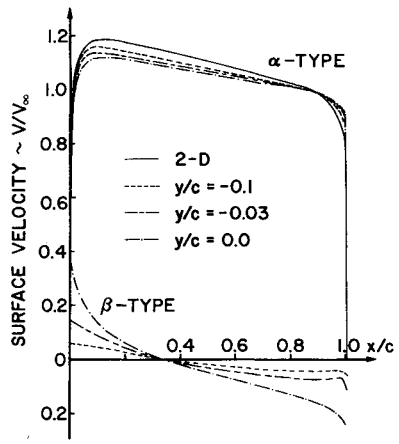

Fig. 5 Chordwise distributions of the α- and β-type surface vorticity strengths on a semi-infinite NACA 0012 nonlifting wing.

After the zeroth and the first iterations, the input distribution for the next iteration is taken to be the mean, I_M, of the results of the zeroth and the first iterations. In the light of the behavior of the results of the basic procedure, it is to be expected that I_M will be closer to the converged solution than either the zeroth or the first. The results, *II*, of the second iteration are compared with its input distribution for convergence. The criterion for convergence is, of course, the smallness of the difference of the results of two successive iterations. Every following iteration, when required, is started with an input surface voriticty distribution which is the mean of the two previous distributions.

Results

The chordwise distributions of the α- and β-type vorticity, as computed using the modified procedure, are given in a tabulated form in Appendix C of Ref. 14. One of the salient features of the results is that the values of the third iteration are different from its input distribution by amounts which are less than one-half of 1% on the entire wing except in the first 5% chord length from the leading edge where the differences are between one-half of 1% to a maximum of 2%. The latter can be attributed to relatively sharp changes in the vorticity gradients which are approximated by a few linear segments only. On the contrary, the results of the basic method showed that the difference between the values of the third and the second iterations was of the order of 2% on the entire wing. The typical pattern is shown in Fig. 4 for a representative control point.

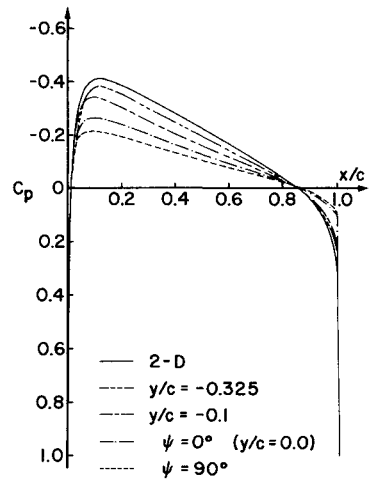

Fig. 6 Chordwise pressure coefficient distributions on the surface of a semi-infinite NACA 0012 wing with half-body-of-revolution tip at zero angle of attack.

The accuracy of the results is checked by computing the normal component of the total velocity vector and it is found to be less than 1% of the freestream value of unity. Three typical chordwise velocity distributions associated with the α- and β-type vorticity distributions are shown in Fig. 5 and compared with the two-dimensional distribution. The negative values of the velocity component associated with β-type voriticity reflect a change of direction of this component aft of the 35% chord location. This is consistent with the bending of the streamlines as required by the geometry of the wing tip. In Fig. 6, the chordwise pressure coefficient distribution is shown for four spanwise locations. The comparison with the result of the two-dimensional flow shows the three-dimensional relief effect of the tip.

It should be pointed out at this stage that in most of the studies,[2-7] the body surface is usually approximated by flat panels and, understandably, that is the simplest and more practical choice for arbitrarily shaped bodies. In the development of the present iterative method, however, only simple geometries are considered and no approximations have been made regarding the curved shapes of the surface elements. Therefore, the results are accurate except for the errors due to the piecewise linear approximation for the vorticity distribution and the truncation errors. This accuracy is achieved at the cost of increased computations in evaluating the integrals for each surface element. A preliminary investigation showed that suitable approximations of the surface elements can reduce the computational effort considerably without noticeable impairment of accuracy. For instance, the surface elements inboard of the tip can be replaced by flat panels formed by joining the corners of the elements and the half-body-of-revolution tip may be divided into half frustrums of cones of axial lengths determined by the adjacent k stations. These approximations simplify the mathematical formulation as some of the integrals can be evaluated analytically and expressed in algebraic form. Consequently, the numerical computations are reduced. A set of approximations which resulted in less than one-tenth of 1% change over the results obtained by using all curved elements is incorporated for the case of finite wing described later. This involves approximating all the curved elements by flat panels, except on the section of the body which contains the control point where the induced velocity is being evaluated. The details are discussed in Ref. 14.

Finite Symmetrical Wing

One of the obvious extensions of the case of the semi-infinite wing is to compute the nonlifting flow on a conventional finite wing. An NACA 0012 wing of aspect ratio

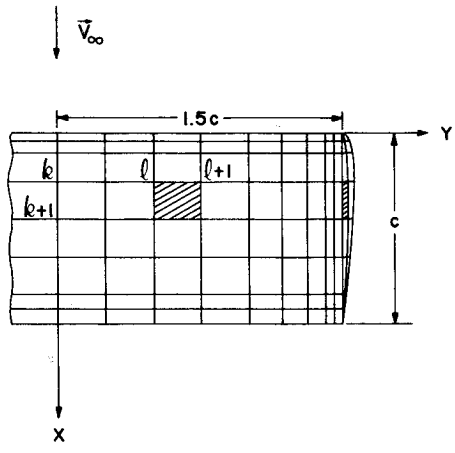

Fig. 7 NACA 0012 wing with half-body-of-revolution tip, AR = 3.

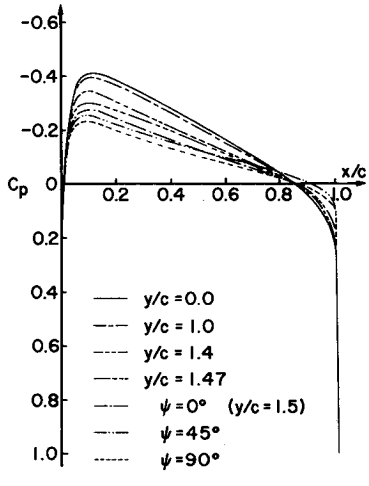

Fig. 8 Chordwise pressure coefficient distributions on the surface of a nonlifting NACA 0012 wing of aspect ratio 3.

three is considered (Fig. 7). The iterations can be carried out from an initial two-dimensional surface voriticity distribution on the entire wing and subsequent application of the modified procedure just outlined. However, a more efficient method will be to start from an initial distribution which is closer to the final solution. This can be accomplished by choosing a surface distribution which, on and near the tip of the finite wing, is the same as the corresponding distribution near the tip of the semi-infinite wing. This choice of initial distribution also affords another advantage. It is obvious that the number of elements on the finite wing will be of the order of twice the number of surface elements on the semi-infinite wing. A considerable saving in computations can be achieved by carrying out two iterations for the semi-infinite case and then transferring to the finite wing. For the case under consideration, the input vorticity distribution used is the same as the input for the third iteration of the semi-infinite case. After one iteration is completed for the finite wing, the results are within one-half of 1% of the input distribution on a major portion of the wing (between the 5% and 75% chord lengths). On the remaining portion, the results differ from the input distribution by approximately 1-3%. The results of the second iteration for the finite wing differ from the corresponding input distribution by less than one-half of 1% on the entire wing and much less than this on a major portion of the wing.[14] The chordwise pressure coefficient distribution on the upper surface of one half of the wing is shown for seven representative locations in Fig. 8. The results show that the major effect of the tip is largely confined to within 20-25% chord length inboard of the tip.

Concluding Remarks

An iterative procedure utilizing a surface vorticity distribution is formulated and developed to compute the three-dimensional nonlifting potential flow on the tip region of a circular cylindrical body with a hemispherical tip. In three iterations, the initial two-dimensional distribution on the entire body is readjusted to give a three-dimensional flow on the tip which merges smoothly with the two-dimensional distribution further inboard from the tip. The difference between the results of the second and third iterations is less than 2%. The results of the iterations exhibit a damped oscillatory pattern of convergence which is also observed for the case of a semi-infinite NACA 0012 wing with half-body-of-revolution tip. This observation leads to a modification of the method to achieve accelerated convergence. The modified procedure is then used to compute nonlifting potential flow on a NACA 0012 wing of aspect ratio three. In each case, a continuous, nearly piecewise linear velocity distribution on the surface is directly obtained from the computed vorticity distribution without further computation.

The most important advantage of the iterative procedure over the more commonly used integral equation formulation is that the surface velocity distribution is obtained without having to solve an extremely large set of linear algebraic equations. The coefficient matrix of the latter which approximates the integral equations of the first kind for the surface vorticity distribution model is usually not well behaved because the diagnonal entries are not dominant.

The logical extension of the present work is to apply the method to a lifting wing. The solution for this case should provide more insight into the problems related with the wing tip vortex. The problem is, however, complicated by the lack of information about the geometry and the vorticity distribution of the trailing vortex system. One of the possible ways to approach the problem is to start the iterative procedure with a surface vorticity distribution on the wing which corresponds to the nonlifting solution with an additional vorticity distribution to account for circulation and lift. Initially, a suitable model for the trailing vortex sheet has to be assumed on which the kinematic boundary condition will have to be satsified. The successive iterations should readjust the vorticity strength distribution on the wing and the trailing vortex system to yield the final solution. The present method may be extended to the case of an arbitrary three-dimensional body in a similar manner. An approximate two-dimensional flow on one cross section of the body may be computed by the method of Ref. 13, assuming that such a condition is appropriate for the body. These results then provide an initial distribution to start the iterative procedure. Alternatively, the two-dimensional vorticity distribution may be computed (e.g., blade- or airfoil-element theory) on predetermined cross sections and the surface vorticity may be assumed to vary linearly between two adjacent elements. The latter approach is being pursued to compute the pressure distribution on a helicopter rotor blade. The results[17] to date indicate that the successive iterations adjust the surface vorticity strengths to give the three-dimensional flow. The final word on the most suitable initial distribution and subsequent convergence must await the completion of further computational studies.

In the course of the present investigation, no approximations are made about the shapes of the curved surface elements. The results, therefore, can provide a basis to check the validity of several possible approximations which can reduce the computational effort considerably. Some preliminary studies resulted in reducing the computational time by more than 50% without a signficant loss of accuracy. However, an extensive numerical evaluation of the relative magnitudes of the contributions to the induced velocity at a control point from various surface elements is needed. It may be possible to entirely omit some of them from the calculations or to express the contribution from some others

as a simple, analytical expression by assuming a uniform constant-strength distribution which is an average of the actual distribution.

References

[1] Lamb, H., *Hydrodynamics,* 6th ed., Dover Publications, Inc., New York, 1945, pp. 58-60.

[2] Hess, J.L. and Smith, A.M.O., "Calculation of Potential Flow about Arbitrary Bodies," *Progress in Aeronautical Sciences,* Vol. 8, ,1967, pp. 1-138.

[3] Hess, J.L., "The Problem of Three-Dimensional Lifting Potential Flow and its Solution by Means of Surface Singularity Distribution," *Computer Methods in Applied Mechanics and Engineering,* Vol. 4, 1974, pp. 283-319.

[4] Hess, J.L., "Improved Solution for Potential Flow about Arbitrary Axisymmetric Bodies by the Use of a Higher Order Surface Source Method," *Computer Methods in Applied Mechanics and Engineering,* Vol. 5, 1975, pp. 297-308.

[5] Woodward, F.A., "An Improved Method for the Aerodynamic Analysis of Wing-Body-Tail Configurations in Subsonic and Supersonic Flow," NASA CR-2228, May 1973.

[6] Pien, P.C., "Calculation of Nonlifting Potential Flow about Arbitrary Three-dimensional Bodies Based on Doublet Distribution," Naval Ship Research and Development Center, Rept. SPD-601-01, Jan. 1975.

[7] Summa, J.N., "Potential Flow About Three-Dimensional Streamlined Lifting Configurations with Application to Wings and Rotors," Stanford University, Stanford, Calif., SUDAAR 485, Sept. 1974.

[8] Prager, W., "Die Druckverteilung an Korpern in ebener Potentialstromung," *Physikalische Zeitschrift,* Vol. XXIV, 1928, p. 865.

[9] Kress, R., "Treatment of Prager Problem of Potential Theory by the Integral Equation Method," *Physics of Fluids,* Supplement II, 1969, pp. 120-125.

[10] Klein, A. and Mathew, J., "Incompressible Potential Flow Solution for Axisymmetric Body-Duct Configurations," *Zeitschrift fur Flugwissenshaften,* Vol. 20, 1972, pp. 221-228.

[11] Grodtkjaer, Erik, "A Direct Integral Equation Method for the Potential Flow about Arbitrary Bodies," *International Journal for Numerical Methods in Engineering,* Vol. 6, Feb. 1973, pp. 253-264.

[12] Milne-Thomson, L.M., *Theoretical Aerodynamics,* 4th ed., Dover Publications, Inc., New York, 1973, pp. 187-188.

[13] Raj, P. and Gray, R.B., "Computation of Two-Dimensional Potential Flow Using Elementary Vortex Distributions," *Journal of Aircraft,* Vol. 15, Oct. 1978. pp. 698-700.

[14] Raj, P., "A Method of Computing the Potential Flow on Thick Wing Tips," Ph.D. Thesis, School of Aerospace Engineering, Georgia Institute of Technology, Atlanta, Ga., 1976, pp. 46-151.

[15] Lotz, I., "Calculation of Potential Flow Past Airship Bodies in Yaw," NACA TM 765, 1932.

[16] Jacobs, E.N., Ward, K.E., and Pinkerton, R.M., "The Characteristics of 78 Related Airfoil Sections from Tests in the Variable-Density Wind Tunnel," NACA Rept. 460, 1933, pp. 299-354.

[17] Shenoy, K.R. and Gray, R.B., private communication, School of Aerospace Engineering, Georgia Institute of Technology, Atlanta, Ga.

From the AIAA Progress in Astronautics and Aeronautics Series . . .

INSTRUMENTATION FOR AIRBREATHING PROPULSION—v. 34

Edited by Allen Fuhs, Naval Postgraduate School, and Marshall Kingery, Arnold Engineering Development Center

This volume presents thirty-nine studies in advanced instrumentation for turbojet engines, covering measurement and monitoring of internal inlet flow, compressor internal aerodynamics, turbojet, ramjet, and composite combustors, turbines, propulsion controls, and engine condition monitoring. Includes applications of techniques of holography, laser velocimetry, Raman scattering, fluorescence, and ultrasonics, in addition to refinements of existing techniques.

Both inflight and research instrumentation requirements are considered in evaluating what to measure and how to measure it. Critical new parameters for engine controls must be measured with improved instrumentation. Inlet flow monitoring covers transducers, test requirements, dynamic distortion, and advanced instrumentation applications. Compressor studies examine both basic phenomena and dynamic flow, with special monitoring parameters.

Combustor applications review the state-of-the-art, proposing flowfield diagnosis and holography to monitor jets, nozzles, droplets, sprays, and particle combustion. Turbine monitoring, propulsion control sensing and pyrometry, and total engine condition monitoring, with cost factors, conclude the coverage.

547 pp. 6 x 9, illus. $14.00 Mem. $20.00 List

TO ORDER WRITE: Publications Dept., AIAA, 1290 Avenue of the Americas, New York, N. Y. 10019